

## ON THE ELECTRON-OPTICAL PHASE SHIFT FOR MAGNETIC NANOPARTICLES

M. Beleggia<sup>1</sup>, S. Tandon<sup>2</sup>, Y. Zhu<sup>1</sup>, and M. De Graef<sup>2</sup>

<sup>1</sup> Materials Science Division, Brookhaven National Laboratory, Upton, NY 11973

<sup>2</sup> Department of Materials Science & Engineering, Carnegie Mellon University, Pittsburgh, PA 15213

The continuously decreasing length scale of magnetic recording media and other applications based on magnetic nanoparticles necessitates the use of advanced characterization methods, both for chemical and structural analysis and for the study of magnetic domains and interactions. Determination of the fine scale magnetic structure is essential for the prediction of various material properties. Lorentz microscopy has for several decades been the dominant observation technique for qualitative magnetic domain observations. A quantum mechanical description of Lorentz images requires knowledge of the magnetic phase shift imparted on the beam electron by the particle and its surrounding fringing field. While such a phase shift is relatively easy to compute for a particle with a high symmetry (e.g., a sphere or circular disk), the situation is more complex for a faceted polyhedral nanoparticle. In the present paper, we introduce a theoretical formalism for determining the magnetic component of the electron-optical phase shift for a polyhedral nanoparticle.

In [1] it was shown that, if the magnetization state  $\mathbf{m} = M_0 \hat{\mathbf{m}}$  of the particle is known, then the vector potential can be calculated analytically in Fourier space. The magnetic phase shift is then given by:

$$\varphi_m(k_x, k_y) = \frac{i\pi B_0}{\phi_0} \frac{D(k_x, k_y, 0)}{k_x^2 + k_y^2} (\hat{\mathbf{m}} \times \mathbf{k})|_z. \quad (1)$$

$\phi_0$  is the flux quantum. The function  $D(\mathbf{k})$  is the particle *shape amplitude*, which, for a faceted particle with  $E$  edges and  $F$  faces, is given by [2]:

$$D(\mathbf{k}) = -\frac{1}{k^2} \sum_{f=1}^F \frac{\mathbf{k} \cdot \mathbf{n}_f}{k^2 - (\mathbf{k} \cdot \mathbf{n}_f)^2} \sum_{e=1}^{E_f} L_{fe} \mathbf{k} \cdot \mathbf{n}_{fe} \text{sinc}\left(\frac{L_{fe}}{2} \mathbf{k} \cdot \mathbf{t}_{fe}\right) e^{-i\mathbf{k} \cdot \boldsymbol{\xi}_{fe}^C}. \quad (2)$$

The various vectors are defined in Fig. 1. We have worked out explicitly the shape amplitude for an isosceles triangular plate and a sheared rectangular plate. From these building blocks, a range of particle shapes can be created, as shown in Fig. 2. The total phase shift is shown in Fig. 3, for a range of particle shapes and magnetization states. The 4 particles on the left (Fig. 3a) have a thickness of 20 nm, the others are 10 nm thick. The saturation induction is  $B_0 = 1$  T. The computational array measures  $512 \times 512$  pixels, with 2 nm per pixel, resulting in a viewing area of  $1 \mu\text{m}^2$ .

Fig. 3b shows the magnetic phase shift  $\varphi_m$  (range  $[-8.10, 5.19]$  rad). The triangular and pentagonal disks have a vortex magnetization state with opposite polarity, and there is no fringing field around these particles. All uniformly magnetized particles (rows 1 and 3) are surrounded by a dipole field; the formalism correctly includes the interactions between these particles through the linearity of the vector potential and resulting phase shift. The two particles in the right-most column have a vortex magnetization state, but there is a weak fringing field around the sharp points of the starshape. The electrostatic phase shift  $\varphi_e$  (range  $[0, 11.01]$  rad) is shown in Fig. 3c. The total phase shift  $\varphi_m + \varphi_e$  and  $\cos 5(\varphi_m + \varphi_e)$  are shown in Fig. 3d and e, resp. (range  $[-3.72, 15.91]$  rad).

Fig. 4 shows simulated Fresnel and Foucault images for the particle arrangement of Fig. 3a. Fig. 4a is the in-focus image for the following imaging parameters: accelerating voltage 200 kV, beam divergence angle  $\theta_c = 10^{-6}$  rad, aperture radius  $2 \text{ nm}^{-1}$ , spherical aberration  $C_s = 1$  m, and defocus spread  $10 \mu\text{m}$ . The normal absorption length is taken to be  $\xi'_0 = 50$  nm. The mean inner potential is  $V_0 = 20$  V. The particles are "supported" by a 20 nm thick amorphous film with a mean inner potential of 10 V. Fig. 4b shows a Fresnel image for a defocus of  $\Delta f = \pm 0.5$  nm. Fig. 4c shows a Foucault image for the indicated aperture shift direction.

We have shown that it is possible to compute the magnetic and electrostatic phase shift components for a wide range of particle shapes. Through the use of isosceles triangular plates and sheared rectangular plates, for which analytical expressions for the shape amplitude  $D(\mathbf{k})$  have been derived, more complex three-dimensional shapes can be built with either a uniform or a vortex magnetization state. Once the phase shift is known in analytical or numerical form, the standard image formation framework for high resolution electron microscopy can be used to compute images for the Fresnel and Foucault imaging modes. This phase computation algorithm introduced opens the way to quantitative phase reconstruction and interpretation for magnetic nanoparticles of arbitrary shape.

References

1. M. Beleggia M. and Y. Zhu, *Phil. Mag. B*, in press (2003); M. Beleggia, S. Tandon. Y. Zhu, and M. De Graef, *Phil. Mag. B*, in press (2003)
2. J. Komrska J., *Optik* 80 (1987) 171.

2. This work was supported by the U.S. Department of Energy, Basic Energy Sciences under contract numbers DE-FG02-01ER45893 and DE-AC02-98CH10886.

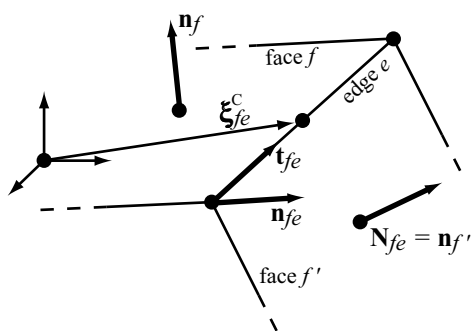


FIG. 1 Schematic illustration of face and edge vectors in Eq. (2).

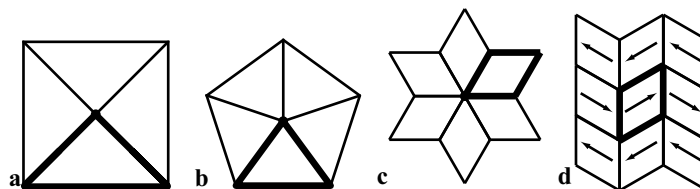


FIG. 2. Various shapes created by rotation and translation of an isosceles triangular plate and a sheared rectangular plate, outlined in thicker lines.

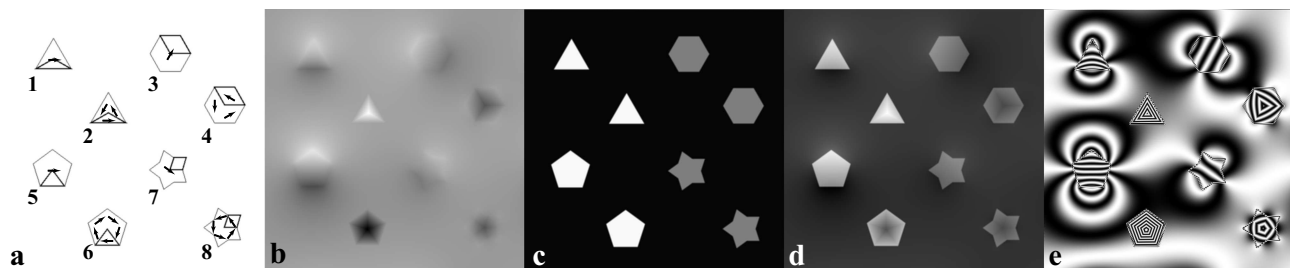


FIG. 3. (a) 8 shapes with various magnetization states; grayscale image of magnetic (b) and electrostatic (c) phase shifts and their sum (d). (e) shows the function  $\cos[5(\phi_e + \phi_m)]$ . Particles with a vortex state have no fringing field, whereas all other particles have a dipole fringing field. Interactions between particles are properly taken into account by the model.

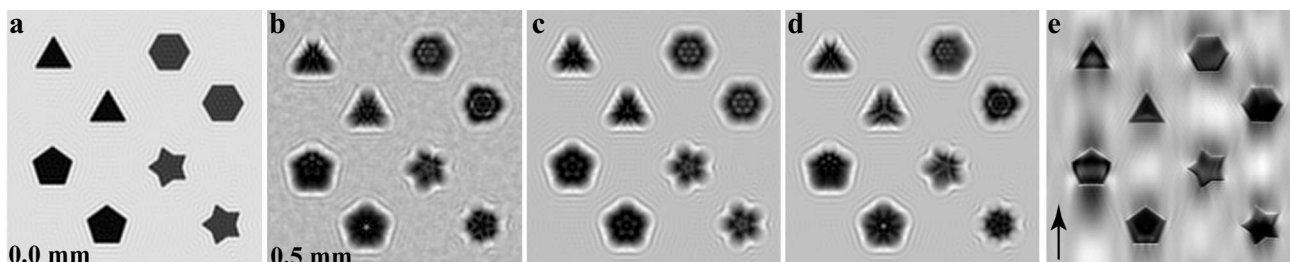


FIG. 4. (a) In-focus image (200 kV) for the particle array of Fig. 3a. (b) over-focus image ( $\Delta f = 0.5$  mm); (c) electrostatic component of image (b), and (d) magnetic component of image (b). (e) is a Foucault image for the indicated aperture shift direction. All images are  $1 \times 1 \mu\text{m}^2$ .